Implementation Strategies for Hyperspectral Unmixing Using Bayesian Source Separation

Frédéric Schmidt, Albrecht Schmidt, Erwan Tréguier, Maël Guiheneuf, Saïd Moussaoui, and Nicolas Dobigeon, *Member, IEEE*

***Abstract*—Bayesian positive source separation (BPSS) is a useful unsupervised approach for hyperspectral data unmixing, where numerical nonnegativity of spectra and abundances has to be ensured, such as in remote sensing. Moreover, it is sensible to impose a sum-to-one (full additivity) constraint to the estimated source abundances in each pixel. Even though nonnegativity and full additivity are two necessary properties to get physically interpretable results, the use of BPSS algorithms has so far been limited by high computation time and large memory requirements due to the Markov chain Monte Carlo calculations. An implementation strategy that allows one to apply these algorithms on a full hyperspectral image, as it is typical in earth and planetary science, is introduced. The effects of pixel selection and the impact of such sampling on the relevance of the estimated component spectra and abundance maps, as well as on the computation times, are discussed. For that purpose, two different data sets have been used: a synthetic one and a real hyperspectral image from Mars.**

***Index Terms*—Bayesian estimation, computation time, hyperspectral imaging, implementation strategy, source separation.**

I. Introduction

IN VISIBLE and near-infrared hyperspectral imaging, each image recorded by the sensor is the solar light reflected and diffused back from the observed planet surface and atmosphere at a particular spectral band. Under some assumptions related to surface and atmosphere properties—e.g., Lambertian surface, no intimate mixture, no diffusion terms in the atmosphere, and homogeneous geometry in the scene—each measured spectrum—i.e., each pixel of the observed image for several spectral bands—is modeled as a linear mixture of the scene component spectra (*endmembers*) [1]–[3]. In this model, the weight of each component spectrum is linked to its abundance in the surface area, which corresponds to the underlying pixel. The main goal of hyperspectral unmixing is to identify the components of the imaged surface and to estimate their respective abundances [4], [5].

By considering P pixels of a hyperspectral image acquired in L frequency bands, the observed spectra are gathered in a $P \times L$ data matrix $\mathbf{X}$, potentially ignoring spatiality. Each row of this matrix contains a measured spectrum at a pixel with spatial index $p = 1, \ldots, P$. According to the linear mixing model, the pth spectrum, i.e., $1 \leq p \leq P$, can be expressed as a linear combination of R pure spectra of the surface components. Using matrix notations, this linear spectral mixing model can be written as

$$\mathbf{X} \approx \mathbf{AS} \tag{1}$$

where nonnegative matrices $\mathbf{A} \in \mathbb{R}_+^{P\times R}$ and $\mathbf{S} \in \mathbb{R}_+^{R\times L}$ approximate $\mathbf{X} \in \mathbb{R}_+^{P\times L}$ in the sense that $1/2\|\mathbf{AS} - \mathbf{X}\|^2$ is minimized ($\mathbb{R}_+^{\cdot\times\cdot}$ denotes the space of matrices with only nonnegative entries of respective dimensions). The rows of matrix $\mathbf{S}$ now contain the pure surface spectra of the R components, and each element a_{pr} of matrix $\mathbf{A}$ corresponds to the abundance of the rth component in pixel with spatial index p. For the qualitative and quantitative descriptions of the observed scene composition, the estimation problem consists of finding matrices $\mathbf{S}$ and $\mathbf{A}$ that allow one to explain the data matrix $\mathbf{X}$ and have a coherent physical interpretation. This approach casts the hyperspectral unmixing as a *source separation* problem under a linear instantaneous mixing model [6]. Source separation is a statistical multivariate data processing problem whose aim is to recover unknown signals (called *sources*) from noisy and mixed observations of these sources [7], [8].

This problem has been studied in-depth in recent years, starting with pioneer work more than 15 years ago [9], [10]. From a statistical point of view, the problem is also related to principal component analysis (PCA) and k-means clustering (see [11] for an overview). Also note that the factorization $\mathbf{AS}$ is not uniquely defined. For instance, for any matrices $\mathbf{Z} \in \mathbb{R}_+^{R\times\cdot}$ such that $\mathbf{ZZ}^{-1} = \mathbf{I}$, then $\mathbf{AZZ}^{-1}\mathbf{S} = (\mathbf{AZ})(\mathbf{Z}^{-1}\mathbf{S}) = \mathbf{A}'\mathbf{S}'$ is a solution as well; this holds even if the minimization is able to find a global minimum. However, when solving this separation problem with hyperspectral data, several constraints can be considered to reduce the set of admissible solutions. A first hard constraint is the nonnegativity of the elements of both

Manuscript received December 14, 2009; revised April 9, 2010. Date of publication September 13, 2010; date of current version October 27, 2010.

F. Schmidt was with the European Space Astronomy Centre, European Space Agency, 28692 Madrid, Spain. He is now with the Laboratoire des Intéractions et Dynamique des Environnements de Surface, UMR 8148, University Paris-Sud, 91405 Orsay, France, and also with the Centre National de la Recherche Scientifique, Université Paris-Sud, 91405 Orsay, France (e-mail: frederic.schmidt@u-psud.fr).

A. Schmidt, E. Tréguier, and M. Guiheneuf are with European Space Astronomy Center, European Space Agency, 28692 Madrid, Spain (e-mail: Albrecht.Schmidt@esa.int; mael.guiheneuf@gmail.com; erwan.treguier@sciops.esa.int).

S. Moussaoui is with the Institut de Recherche en Communication et Cybernétique de Nantes (IRCCyN), Centre National de la Recherche, UMR 6597, École Centrale Nantes, 44321 Nantes Cedex 3, France (e-mail: said.moussaoui@irccyn.ec-nantes.fr).

N. Dobigeon is with the Institut de Recherche en Informatique de Toulouse (IRIT), and with the Institut National Polytechnique de Toulouse, and the Ecole Nationale Supérieure d'Electrotechnique, d'Electronique, d'Hydraulique et d'Informatique, et des Télécommunications (ENSEEIHT), and also with the Telecommunications for Space and Aeronautics TeSA, University of Toulouse, 31071 Toulouse Cedex 7, France (e-mail: Nicolas.Dobigeon@enseeiht.fr).

Color versions of one or more of the figures in this paper are available online at http://ieeexplore.ieee.org.

Digital Object Identifier 10.1109/TGRS.2010.2062190

matrices $\mathbf{S}$ and $\mathbf{A}$ since they correspond to pure spectra and abundances of the surface components, respectively. A second constraint that may be imposed is the sum-to-one (additivity) constraint of the abundances. Indeed, the abundance weights correspond to proportions and should therefore sum to unity.

Several algorithms have been proposed in the literature to solve fully constrained unmixing problems, i.e., handling both of the constraints imposed on the spectra and abundances. Specifically, an iterative algorithm called iterated constrained endmembers (ICE) has been proposed in [12] to minimize the size of the simplex formed by the estimated endmembers. However, as noted in [13], results provided by ICE strongly depend on the choice of the algorithm parameters. More recently, Jia and Qian have developed in [14] complexity-based BSS algorithms that exploit pixel correlations to recover endmember signatures. In [15], Miao and Qi have introduced a nonnegative matrix factorization (NMF) algorithm with an additivity penalty on the abundance coefficients. Similarly, other constrained NMF approaches exploiting smoothness and sparseness features have been considered in [16]. Note that all the strategies described earlier are based on an optimization scheme to minimize a penalty criterion. Consequently, they may suffer from convergence issues, e.g., due to the presence of local maxima and the large number of parameters to be estimated.

Alternatively, the constrained separation problem can be conveniently addressed in a Bayesian framework. Two algorithms that perform unsupervised separation under positivity and sum-to-one constraints have been recently proposed [17], [18]. These algorithms are based on hierarchical Bayesian modeling to encode prior information regarding the observation process the parameters of interest and include the positivity and full additivity constraints. The complexity of the inference from the posterior distribution of the parameters of interest is tackled using Markov chain Monte Carlo (MCMC) methods [19], [20], which has been proposed to analyze hyperspectral images [21]. The algorithmic details are not described here. The reader is invited to read the pseudocodes summarized in algorithms 1 and 2 and to consult [17] and [18] for further details. The only difference between the two Bayesian positive source separation (BPSS) algorithms is the sampling of the abundance vectors $\mathbf{a}_p$ $(p = 1, \ldots, P)$. However, since these algorithms rely on MCMC methods, the computation time drastically increases with the image size, and these algorithms have not been applied for large-scale data processing in spite of their high effectiveness.

The aim of this paper is to discuss some implementation strategies that allow one to apply these algorithms to real hyperspectral data even if images are large. Previous works about blind source separation of hyperspectral images have been proposed [22]–[24], but only few use positivity/sum-to-unity constraints [25]. To overcome this difficulty, a first approach has been proposed in [25] to combine independent component analysis (ICA) and BPSS. First, applying an ICA algorithm (such as JADE [26] or FastICA [27]) to hyperspectral images is applied to get a rough spatial classification of the scene and to sample relevant pixels (i.e., from each *class*, the pixels whose spectra are mostly uncorrelated are selected). Second, the spectra associated to these pixels will serve in the Bayesian separation algorithm to estimate the endmember spectra. Finally, the abundances can then be estimated on the whole image using the estimated spectra. However, this strategy presents a limitation related to the difficulty to determine the number of pixels to retain from each independent component class. In this paper, another pixel selection strategy based on the computation of the convex hull of the hyperspectral data is introduced. Its influence on separation performances is also discussed. The issue of estimating the number of sources, or "intrinsic dimension" [28], will not be addressed in this paper. Several methods have been proposed in the literature [29], [30].

This paper is organized as follows. Section II describes the proposed implementation strategies adopted for this paper. Section III summarizes the improvements related to the technical aspects of memory storage and computation issues. Section IV discusses the performances of the resulting algorithms when the pixel selection preprocessing step is introduced.

Algorithm 1 BPSS algorithm

for $i = 1, \ldots, N_{\mathrm{MC}}$ **do**
% sampling the abundance hyperparameters
for $p = 1, \ldots, P$ **do**
Draw λ_p from the pdf

$$f(\lambda_p|\mathbf{a}_{p:}, \gamma_p) \propto \prod_{r=1}^{R} \left[\frac{\gamma_p^{\lambda_p}}{\Gamma(\lambda_p)} a_{p,r}^{\lambda_p} \right] e^{-\epsilon\lambda_p} \mathbf{1}_{\mathbb{R}+}(\lambda_p).$$

end for
% sampling the abundance hyperparameters
for $p = 1, \ldots, P$ **do**
Draw γ_p from the gamma distribution

$$\gamma_p|\lambda_p, \mathbf{a}_{p:} \sim \mathcal{G}\left(1 + R\lambda_p + \epsilon, \sum_{r=1}^{R} a_{p,r} + \epsilon\right).$$

end for
% sampling the abundance vectors
for $p = 1, \ldots, P$ and $r = 1, \ldots, R$ **do**
Draw $a_{p,r}$ from the pdf

$$f\left(a_{p,r}|\lambda_p, \gamma_p, \mathbf{S}, \boldsymbol{\sigma}_{\mathrm{e}}^2, \mathbf{X}\right) \propto a_{p,r}^{\lambda_r - 1} \mathbf{1}_{\mathbb{R}+}(a_{p,r}) \exp\left[-\frac{(a_{p,r} - \mu_{p,r})^2}{2\delta_p^2} - \gamma_p a_{p,r}\right]$$

end for
% sampling the noise hyperparameters
Draw ψ_{e} from the inverse-gamma distribution

$$\psi_{\mathrm{e}}|\boldsymbol{\sigma}_{\mathrm{e}}^2, \rho_{\mathrm{e}} \sim \mathcal{IG}\left(\frac{P\rho_{\mathrm{e}}}{2}, \frac{1}{2}\sum_{p=1}^{P} \frac{1}{\sigma_{\mathrm{e},p}^2}\right).$$

% sampling the noise variances
for $p = 1, \ldots, P$ **do**
Draw $\sigma_{\mathrm{e},p}^2$ from the inverse-gamma distribution

$$\sigma_{\mathrm{e},p}^2|\psi_{\mathrm{e}}, \mathbf{a}_{p:}, \mathbf{S}, \mathbf{x}_{p:} \sim \mathcal{IG}\left(\frac{\rho_{\mathrm{e}} + L}{2}, \frac{\psi_{\mathrm{e}} + \|\mathbf{x}_{p:} - \mathbf{S}\mathbf{a}_{p:}\|^2}{2}\right).$$

end for
% sampling the source hyperparameters
for $r = 1, \ldots, R$ **do**

Draw α_r from the pdf

$$f(\alpha_r|\mathbf{s}_{r:},\beta_r) \propto \prod_{l=1}^{L}\left[\frac{\beta_r^{\alpha_r}}{\Gamma(\alpha_r)}s_{r,l}^{\alpha_r}\right]e^{-\epsilon\alpha_r}\mathbf{1}_{\mathbb{R}^+}(\alpha_r).$$

end for
% sampling the source hyperparameters
for $r = 1,\ldots,R$**do**
Draw β_r from the gamma distribution

$$\beta_r|\alpha_r,\mathbf{s}_{r:} \sim \mathcal{G}\left(1+L\alpha_r+\epsilon, \sum_{l=1}^{L}s_{r,l}+\epsilon\right).$$

end for
% sampling the source spectra
for $r = 1,\ldots,R$ and $l = 1,\ldots,L$**do**
Draw $s_{r,l}$ from the pdf

$$f\left(s_{r,l}|\alpha_r,\beta_r,\mathbf{A},\boldsymbol{\sigma}_{\mathrm{e}}^2,\mathbf{X}\right) \propto s_{r,l}^{\alpha_r-1}\mathbf{1}_{\mathbb{R}^+}(s_{r,l})\exp\left[-\frac{(s_{r,l}-\mu_{r,l})^2}{2\delta_r^2}-\beta_r s_{r,l}\right]$$

end for
end for

Algorithm 2 Fully constrained BPSS algorithm (BPSS2)

for $i = 1,\ldots,N_{\mathrm{MC}}$**do**
% sampling the abundance vectors
for $p = 1,\ldots,P$**do**
Draw $\mathbf{a}_{p:}$ from the pdf

$$f\left(\mathbf{a}_{p:}|\mathbf{A},\boldsymbol{\sigma}_{\mathrm{e}}^2,\mathbf{X}\right) \propto \exp\left[-\frac{1}{2}(\mathbf{a}_{p:}-\boldsymbol{\mu}_p)^{\mathsf{T}}\boldsymbol{\Lambda}_p^{-1}(\mathbf{a}_{p:}-\boldsymbol{\mu}_p)\right]\mathbf{1}_{\mathbb{S}}(\mathbf{a}_{p:})$$

with

$$\mathbb{S} = \left\{\mathbf{a}_{p:}a_{p,r} \geq 0,\ \forall r = 1,\ldots,R,\ \sum_{r=1}^{R}a_{p,r} = 1\right\}.$$

end for
% sampling the noise hyperparameters
Draw ψ_{e} from the inverse-gamma distribution

$$\psi_{\mathrm{e}}|\boldsymbol{\sigma}_{\mathrm{e}}^2,\rho_{\mathrm{e}} \sim \mathcal{IG}\left(\frac{P\rho_{\mathrm{e}}}{2},\frac{1}{2}\sum_{p=1}^{P}\frac{1}{\sigma_{\mathrm{e},p}^2}\right).$$

% sampling the noise variances
for $p = 1,\ldots,P$**do**
Draw $\sigma_{\mathrm{e},p}^2$ from the inverse-gamma distribution

$$\sigma_{\mathrm{e},p}^2|\psi_{\mathrm{e}},\mathbf{a}_{p:},\mathbf{S},\mathbf{x}_{p:} \sim \mathcal{IG}\left(\frac{\rho_{\mathrm{e}}+L}{2},\frac{\psi_{\mathrm{e}}+\|\mathbf{x}_{p:}-\mathbf{S}\mathbf{a}_{p:}\|^2}{2}\right).$$

end for
% sampling the source hyperparameters
for $r = 1,\ldots,R$ **do**
Draw α_r from the pdf

$$f(\alpha_r|\mathbf{s}_{r:},\beta_r) \propto \prod_{l=1}^{L}\left[\frac{\beta_r^{\alpha_r}}{\Gamma(\alpha_r)}s_{r,l}^{\alpha_r}\right]e^{-\epsilon\alpha_r}\mathbf{1}_{\mathbb{R}^+}(\alpha_r).$$

end for
% sampling the source hyperparameters
for $r = 1,\ldots,R$**do**
Draw β_r from the gamma distribution

$$\beta_r|\alpha_r,\mathbf{s}_{r:} \sim \mathcal{G}\left(1+L\alpha_r+\epsilon, \sum_{l=1}^{L}s_{r,l}+\epsilon\right).$$

end for
% sampling the source spectra
for $r = 1,\ldots,R$ and $l = 1,\ldots,L$**do**
Draw $s_{r,l}$ from the pdf

$$f\left(s_{r,l}|\alpha_r,\beta_r,\mathbf{A},\boldsymbol{\sigma}_{\mathrm{e}}^2,\mathbf{X}\right) \propto s_{r,l}^{\alpha_r-1}\mathbf{1}_{\mathbb{R}^+}(s_{r,l})\exp\left[-\frac{(s_{r,l}-\mu_{r,l})^2}{2\delta_r^2}-\beta_r s_{r,l}\right]$$

end for
end for

II. Optimization Strategies

The optimization consists of two independent parts, which will be referred to as follows: 1) *technical optimization (TO)* to reduce the memory footprint, lower the average cost of algorithmic operations, and make smarter reuse of memory, and 2) *convex hull optimization (CHO)* to reduce the number of spectra to be processed.

Both parts enabled us to analyze hyperspectral images that so far were not open to analysis. The authors stress that the techniques applied in 1) do not alter the results of the original algorithm (see Section III). On the other hand, the optimization strategy 2) only selects a subset of the original input and may therefore change the results. The impact of the strategy 2) needs to be evaluated, which will be presented in Section IV.

A. TO

The algorithms introduced in [17] and [18] and referred to as BPSS and BPSS2, respectively, could be successfully launched on an image of a restricted size, typically of a few thousand pixels. The main goal of this paper is to optimize the memory requirement of these algorithms to process a whole hyperspectral image of 100 000 spectra, as it typically occurs in earth and planetary science. Since the time requirements of the computation increase drastically for a larger number of pixels and a larger number of sources, another challenging objective is to reduce as much as possible the computation time. In that respect, our proposal is to discuss the memory storage, the data representation, the operating system (OS) architecture, and the computing parallelization. These algorithms have been implemented in MATLAB for this paper, but future implementations will be done in other languages as well.

1) Memory: Thanks to the MATLAB profiler, it can be noticed that the main limitation of the BPSS implementation is the contiguous memory. Fragmentation may occur when variables are resized after memory allocation. In this case, the memory management might not be able to allocate a chunk of memory that is large enough to hold the new variable.

TABLE I
SUMMARY OF MEMORY LIMITATION, DEPENDING ON THE OS

Operating System	Memory Limitation
32-bit Microsoft Windows XP Windows Vista	2GB
32-bit Windows XP with 3 GB *boot.ini* switch 32-bit Windows Vista with *increaseuserva* set	3GB
32-bit LINUX	3GB
64-bit Windows XP, Linux, Apple Macintosh OS X or SunSolaris running 32-bit MATLAB©	4GB
64-bit Windows XP, Windows Vista, Linux, or Solaris running 64-bit MATLAB©	8GB

TABLE II
COMPUTATION TIMES (AFTER TO) IN SECONDS, FOR A SYNTHETIC DATA SET WITH THREE ENDMEMBERS (NO CUTOFF, NO NOISE), FOR BOTH BPSS AND BPSS2, WITH AND WITHOUT CHO. IN THIS EXAMPLE, 944 PIXELS WERE SELECTED FORTHE CHO AMONG A TOTAL OF 100 000. THE NAME OFTHE RUN OF TABLE III AND TABLE IV IS NOTED IN PARENTHESIS

Algorithm	Without CHO	With CHO	Time ratio
BPSS	71463 (BPSS-2)	2205 (BPSS-1)	32.41
BPSS2	530654 (BPSS2-2)	7133 (BPSS2-1)	74.39

Significant garbage collection may set in, which may have a significant performance impact. In our case, to reduce the impact of garbage collection, preallocating the matrices and work with global variables has been found to be useful.

2) Precision: MATLAB, by default, computes on double precision. However, computing with single data type saves a lot of computation time while providing sufficient arithmetic precision. It has been estimated to win up to 60% computation time on an x86 processor architecture, while the changes to the code have been minimal. Furthermore, most data sets come as single precision.

3) OS Architecture: It is interesting to note that MATLAB is limited in terms of memory usage (regardless of the size of physical memory). This depends on the OS and the MATLAB version (see Table I).

Therefore, a 32-bit LINUX architecture has been chosen.

4) Parallelization: MATLAB contains libraries dedicated to automatically parallelize parts of the algorithms on a single computer. BPSS has been run on a four-core machine. The underlying matrix libraries already provide a certain level of parallelism, depending on the number of available cores. However, in the future, parts of the code could be parallelized, and the jobs could be submitted to a grid in order to speed up the calculation process.

B. CHO

The proposed pixel selection strategy is based on the convex hull of the data matrix projection into the subspace spanned by the principal components. The convex hull of a point set is the smallest convex set that includes all the points [31]. The pixels associated to the vertices of the convex hull are selected [32] and are expected, despite their limited number, to exhibit the main spectral features of the whole data set. In terms of abundances, this sample of points should contain the pixels with the highest abundances of the components that contribute to the investigated hyperspectral image (i.e., the purest pixels or most extreme pixels). It can be used as a concise representation of the data set that still features the strongest spectral signatures available in the original image. This strategy is also used as a first step in endmember extraction algorithms for dimension reduction and purest pixel determination [32]–[37]. Pixel selection has the advantage to reduce the number of mixture spectra to unmix and to enforce the sparsity of the mixing coefficients to be estimated. Note that the spectral dimension of the selected spectra is not changed; only the spatial dimension is reduced since only a few pixels are selected.

The convex hull selection has been implemented after seven spectral components have been selected through PCA, which turned out to be a good compromise between resource consumption and accuracy.

III. PERFORMANCE AND ACCURACY OF TO

All the following runs are performed on a Quad-Core AMD Opteron Processor 8384 at 2.7 GHz with 2 GB of memory.

1) Performance: Computation times between the previous version of BPSS and the TO version have been compared when processing a synthetic data set of 1052 spectra of 128 bands and 3 sources. For a run attempting at estimating three sources, the computation time has decreased from 1106 s (previous version) to 724 s (TO version), i.e., by a factor of about 1.5. In addition, the total memory consumption is nearly half for the TO version of the algorithm.

2) Accuracy: Due to the stochastic nature of the BPSS algorithms, it is difficult to demonstrate that two algorithms are semantically identical. In order to check that no significant loss of accuracy has been induced by TO and, in particular, by the change from double to single precision, several tests have been performed with different random seeds χ_1 and χ_2, which are used for the initialization step of the MCMC. The sources $S_{\chi 1}$ and $S_{\chi 2}$ estimated with and without TO have been compared.

The average correlations between $S_{\chi 1}$ and $S_{\chi 2}$ are 0.9816 ± 0.0315 and 0.9818 ± 0.0255 without and with TO, respectively. These correlations are due to the stochastic approach in the Bayesian framework. Correlation values are similar, indicating that the stochastic variance has not been affected by TO.

The average cross correlation between $S_{\chi 1}$ and $S_{\chi 2}$ with and without TO is 0.9760 ± 0.0388. This value is similar to the correlation due to the stochastic process, demonstrating that the TO version is equivalent to the original version of BPSS.

No significant differences have been observed, confirming that the TO version is equivalent to the original version of BPSS.

IV. PERFORMANCE AND ACCURACY OF CHO

The impact of the convex hull pixel selection preprocessing step has been evaluated on two data sets: 1) synthetic data generated from linear mixtures of known materials and 2) an Observatoire pour la Minéralogie, l'Eau, les Glaces et l'Activité (OMEGA) hyperspectral image of the south polar cap of Mars as an example from planetology. Since the BPSS with TO has been shown to be semantically equivalent to the previous version, the TO approach is used in the rest of this paper.

TABLE III
RESULTS OBTAINED FOR DIFFERENT SYNTHETIC DATA SETS WITH THE BPSS ALGORITHM. THE CHARACTERISTICS OF EACH DATA SET ARE SHOWN: NUMBER OF ENDMEMBERS, CUTOFF, AND NOISE. EACH DATA SET HAS BEEN ANALYZED WITH A NUMBER OF SOURCES TO BE ESTIMATED EQUAL TO THE NUMBER OF ENDMEMBERS USED TO GENERATE THE ARTIFICIAL DATA SET, WITH AND WITHOUT PIXEL SELECTION. THE QUALITY OF THE ESTIMATION IS EXPRESSED THROUGH THE NUMBER OF WELL-ESTIMATED SOURCES AND THE MEAN ABSOLUTE EXPRESSION, AS EXPLAINED IN THE TEXT

Run Id	Cutoff (%)	Nb of endmembers	Noise	Pixel selection	Nb of well-estimated sources	Mean correlation (%)
BPSS-1	100%	3	no	yes	2/3	99.9441
BPSS-2	100%	3	no	no	2/3	99.9963
BPSS-3	80%	3	no	yes	2/3	98.5826
BPSS-4	80%	3	no	no	2/3	99.9286
BPSS-5	60%	3	no	yes	2/3	98.2135
BPSS-6	60%	3	no	no	2/3	99.2499
BPSS-7	100%	5	no	yes	2/5	92.0689
BPSS-8	100%	5	no	no	3/5	92.5181
BPSS-9	100%	10	no	yes	5/10	88.3081
BPSS-10	100%	10	no	no	6/10	94.2996
BPSS-11	100%	3	OMEGA	yes	2/3	99.9067
BPSS-12	100%	3	OMEGA	no	2/3	99.9961
BPSS-13	100%	3	10xOMEGA	yes	2/3	99.8927
BPSS-14	100%	3	10xOMEGA	no	2/3	99.9976
BPSS-15	100%	3	100xOMEGA	yes	2/3	98.8182
BPSS-16	100%	3	100xOMEGA	no	2/3	98.2574
BPSS-17	ices: 100%, alb.: 35%	3	no	yes	2/3	99.9811
BPSS-18	ices: 100%, alb.: 35%	3	no	no	2/3	98.9855

A. Synthetic Data

1) Description: Several synthetic data sets have been generated by mixing a known number of endmembers, with abundances simulated with uniform distribution. The generated data sets are of size 200 $\times$ 500 pixels, which is a spatial size similar to the one of a typical hyperspectral image. For the endmembers, the following spectra have been used: H_2O and CO_2 ice spectra [38], [39] and mineral spectra from the U.S. Geological Survey Digital Spectral Library splib06a [40], resampled to match the 128 wavelengths of OMEGA C Channel [41]. To ensure the sum-to-one constraint on the R endmember abundances, a uniform distribution on the simplex has been used following a well-established scheme [42]. Synthetic data sets have been generated with three, five, and ten endmembers. Based on this method, data sets for which the maximum abundance of each single endmember was limited to certain values (100%, 80%, and 60%) have also been considered. These latter data, which are called "cutoff" in the sequel, allow one to test the method efficiency face to various conditions in terms of purity of the samples (in cases where pure—to a certain degree—components occur in the data set or not). In addition, a three-component asymmetric data set has been investigated, with one of the component abundances (albite) being limited to a cutoff of 35% and the abundances of the two others (ices) not being limited. In addition, data sets with some added OMEGA-like Gaussian noise, amplified or not, have also been generated and investigated. The noise estimation on the dark currents of the OMEGA instruments for observation 41_1 has been used [39]. Note that, for all the considered simulation scenarios, the number of sources to be estimated has been tuned to the actual number of endmembers used to produce the artificial data set.

2) Performance: Computation times are about 50 times shorter when pixel selection by convex hull (CHO) is performed as a preprocessing step (see Table II).

3) Accuracy:

a) Analysis of the results: The spectrum of each estimated source has been compared to the spectra from the spectral library containing the pure endmembers used to produce the synthetic data set. The absolute value of the correlation has been used as a similarity measurement (thus as a criterion for the determination of the best spectral match). In Fig. 1, each source is represented along with its best match, according to the aforementioned criterion. Table III (resp. Table IV) shows the results for BPSS (resp. BPSS2).

A source is considered a good estimation of a certain endmember if both spectrally match each other best and if their absolute correlation is greater than 80%. For each run, the number of well-estimated sources is mentioned in Tables III and IV. Note that endmembers matched by several sources, in case it happens, are only counted once. Along with the number of well-estimated sources, the mean value of the correlations between (only) the well-estimated sources and their best spectral match also helps for the assessment of the accuracy for the estimation of the whole set of sources for each run. Simple distance could not be used here because the scale in usual blind source separation is undetermined [8].

b) BPSS versus BPSS2: In most of the tested cases, the quality of estimation is unambiguously better with BPSS2 than that with BPSS (see Tables III and IV). The improvement appears to be even more significant when the number of endmembers is increasing. Our three-endmember test data set is a mixture of two endmembers with strong spectral signatures (CO_2 and H_2O ices) and a third one with weaker signatures (albite), as often with minerals. Interestingly, while using BPSS allows one to correctly estimate the ice spectra but not albite, BPSS2 is actually able to correctly estimate the three endmembers. This confirms that adding the sum-to-one constraint is necessary when dealing with such a data set, which is important regarding the analysis of other data set.

c) Effect of the pixel selection (CHO): With the exception of the asymmetric data set (see in the following), the endmembers are less well estimated when a pixel selection has been performed, with the loss appearing to be less significant when the number of endmembers is low.

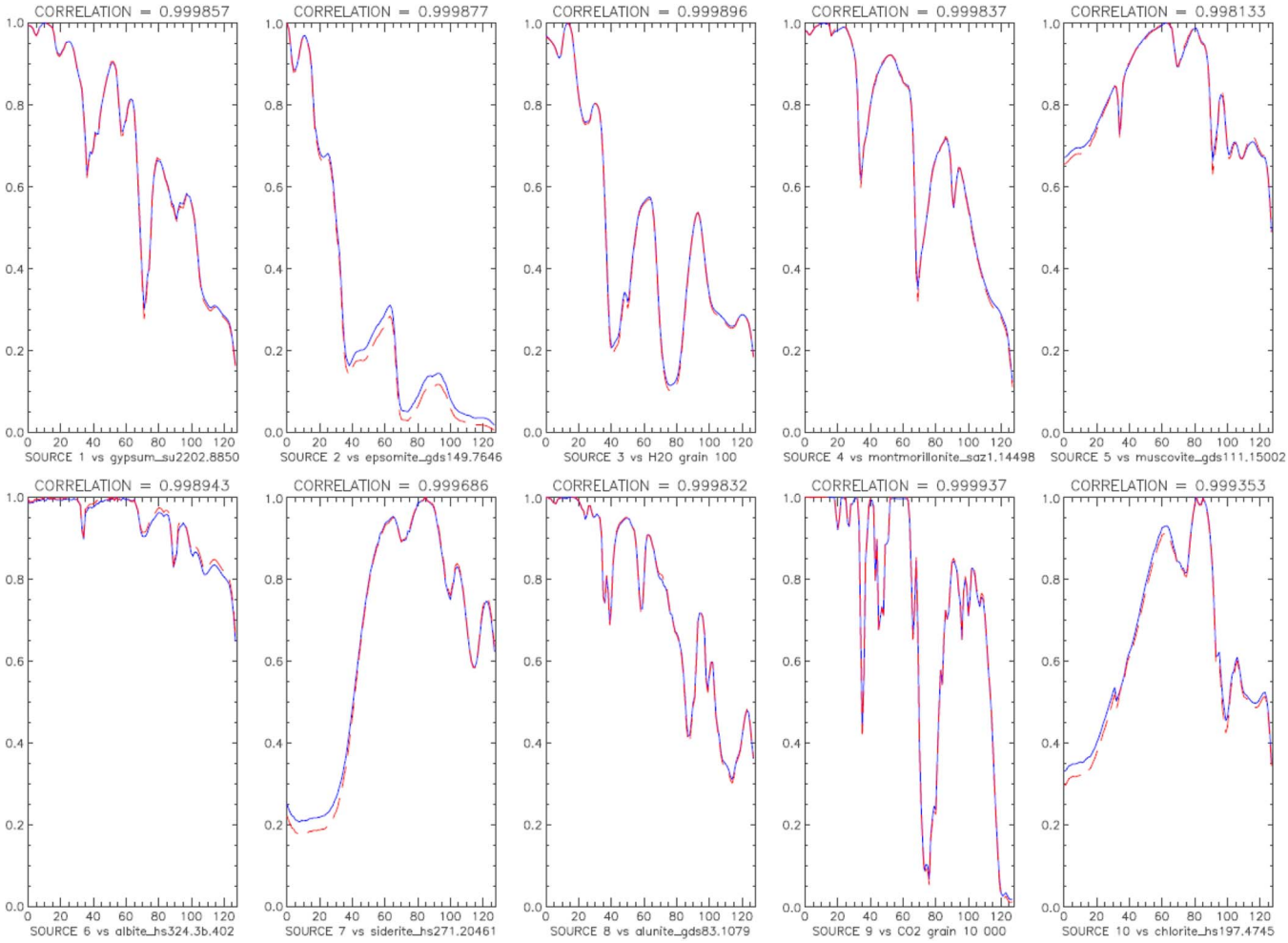

Fig. 1. (Blue lines) Sources estimated by BPSS2 and (red dotted lines) their spectral matches for an artificial data set with ten endmembers (no cutoff, no noise).

TABLE IV
RESULTS OBTAINED FOR DIFFERENT SYNTHETIC DATA SET WITH THE BPSS2 ALGORITHM. THE CHARACTERISTICS OF EACH DATA SET ARE SHOWN: NUMBER OF ENDMEMBERS, CUTOFF, AND NOISE. EACH DATA SET HAS BEEN ANALYZED WITH A NUMBER OF SOURCES TO BE ESTIMATED EQUAL TO THE NUMBER OF ENDMEMBERS USED TO GENERATE THE ARTIFICIAL DATA SET, WITH AND WITHOUT PIXEL SELECTION. THE QUALITY OF THE ESTIMATION IS EXPRESSED THROUGH THE NUMBER OF WELL-ESTIMATED SOURCES AND THE MEAN ABSOLUTE EXPRESSION, AS EXPLAINED IN THE TEXT

Run Id	Cutoff (%)	Nb of endmembers	Noise	Pixel selection	Nb of well estimated sources	Mean correlation (%)
BPSS2-1	100%	3	no	yes	3/3	99.8923
BPSS2-2	100%	3	no	no	**3**/3	99.9222
BPSS2-3	80%	3	no	yes	2/3	95.8934
BPSS2-4	80%	3	no	no	**3**/3	99.9200
BPSS2-5	60%	3	no	yes	2/3	95.2965
BPSS2-6	60%	3	no	no	3/3	97.5408
BPSS2-7	100%	5	no	yes	3/5	99.2821
BPSS2-8	100%	5	no	no	**5**/5	99.9174
BPSS2-9	100%	10	no	yes	5/10	98.9439
BPSS2-10	100%	10	no	no	10/10	99.9535
BPSS2-11	100%	3	OMEGA	yes	3/3	99.8726
BPSS2-12	100%	3	OMEGA	no	3/3	99.9955
BPSS2-13	100%	3	10xOMEGA	yes	3/3	99.7298
BPSS2-14	100%	3	10xOMEGA	no	3/3	99.9962
BPSS2-15	100%	3	100xOMEGA	yes	2/3	95.4706
BPSS2-16	100%	3	100xOMEGA	no	3/3	98.5647
BPSS2-17	ices: 100%, alb.: 35%	3	no	yes	3/3	95.9402
BPSS2-18	ices: 100%, alb.: 35%	3	no	no	2/3	99.7202

Also note that the results with pixel selection do not appear to be very sensitive to the cutoff variations: The loss of quality (between runs performed with and without pixel selection) is similar for cutoffs of 60%, 80%, and 100%, which can be explained by the pixel selection's ability to extract the purest available pixels.

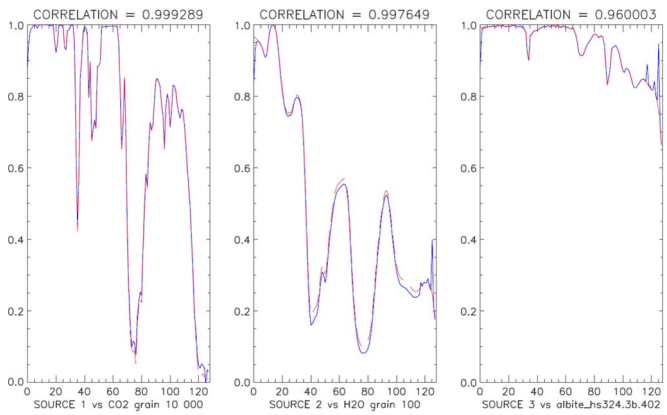

Fig. 2. (Blue lines) Sources estimated by BPSS2 and (red dotted lines) their spectral matches for an artificial data set with three endmembers and 100-times amplified OMEGA-like noise (no cutoff).

d) Effect of the number of endmembers: Due to the curse of dimensionality, the higher the number of endmembers to be estimated with a fixed number of wavelengths, the more difficult the estimation becomes [43], [44]. Still, BPSS2 gives excellent results even for ten sources, as all spectra are estimated with a correlation coefficient higher than 99% (see Fig. 1).

e) Effect of the maximum abundance cutoff: The cutoff affects the quality of estimation, which is clearly better, for BPSS and BPSS2, when pure components occur in the data set. This has to be remembered when dealing with real data sets.

f) Effect of noise: The results clearly show that the method is very robust to noise, as the estimation of the sources does not appear to be significantly affected by the addition of a Gaussian OMEGA-like noise to the synthetic data set. BPSS2 (without pixel selection) even manages to successfully overcome the addition of a 100-times amplified OMEGA-like noise (see Table II and Fig. 2).

g) Effect of asymmetry in maximum abundance cutoff: In this case, the results are better with pixel selection rather than without. BPSS2 with pixel selection is the only run (performed on this synthetic data set) that allows one to successfully estimate the three endmembers that have been used to generate the data set, including albite, whose abundances have been limited to a cutoff of 35% and whose spectral signature is weaker than the ones of the other endmembers (ices). This result can be explained by the fact that pixel selection is able to extract the pixels with the strongest available albite signature, and consequently overcomes the blinding effect of the ices occurring in the whole data set, which has affected the results when no pixel selection has been performed.

B. OMEGA Data

1) Presentation: The OMEGA instrument is a spectrometer onboard Mars Express (European Space Agency), which provides hyperspectral images of the Mars surface, with a spatial resolution from 300 m to 4 km, 96 channels in the visible range, and 256 wavelength channels in the near infrared [45]. In this paper, 184 spectral bands have been selected according to the best signal-to-noise ratio. Conversely, spectral bands that contain thermal emission have been removed.

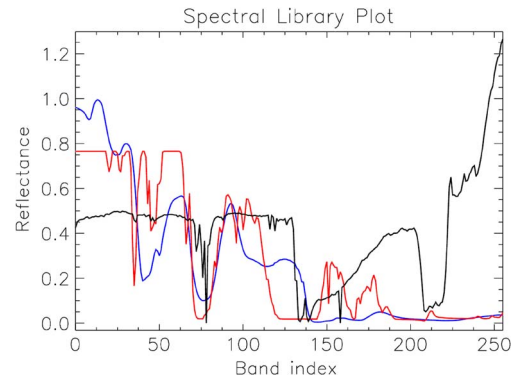

Fig. 3. Reference spectra of the OMEGA hyperspectral image 41_1: (i) in blue: synthetic H_2O ice with a grain size of 100 μm, (ii) in red: synthetic CO_2 ice with a grain size of 10 cms, and (iii) in black: OMEGA typical dust materials with atmosphere absorption.

TABLE V
COMPUTATION TIMES IN SECONDS, FOR THE OMEGA 41_1 IMAGE WITH THREE ENDMEMBERS, FOR BOTH BPSS AND BPSS2, WITH AND WITHOUT CHO. IN THIS EXAMPLE, 670 PIXELS HAVE BEEN SELECTED WITH THE CHO, AMONG A TOTAL OF 111 488. THE NAME OF THE RUN OF TABLE VI IS NOTED IN PARENTHESES

Algorithm	Without CHO	With CHO	Time ratio
BPSS	166 400 (OMEGA-5)	1 468 (OMEGA-7)	113.28
BPSS2	332 680 (OMEGA-6)	3 176 (OMEGA-8)	104.71

TABLE VI
RESULTS ON ALGORITHMS BPSS AND BPSS2 ON A PORTION OF THE OMEGA IMAGE (41_1.CUT) AND ON THE ENTIRE IMAGE (41_1). FOR 41_1.CUT, THE PROPORTION OF PIXELS WITH DETECTED CO_2 IS 48.72%, AND IT IS 63.48% FOR H_2O [39]. FOR 41_1, THE PROPORTIONS OF PIXELS FOR CO_2 AND H_2O ARE 16.76% AND 21.84%, RESPECTIVELY. THE COLUMNS H_2O, CO_2, AND DUST INDICATE THE CORRELATIONS COEFFICIENT BETWEEN THE ESTIMATED SOURCES AND THE REFERENCE SPECTRA. (−) INDICATES NO IDENTIFICATION OF H_2O NEITHER FROM SPECTRAL NOR SPATIAL RESULTS. THIS SOURCE HAS BEEN DETECTED TO BE CO_2 ICE (CORRELATION OF 0.911)

Run Id	Image	Algo	pixel selection	H_2O	CO_2	dust
OMEGA-1	41_1.CUT	BPSS	no	0.883	0.955	0.542
OMEGA-2	41_1.CUT	BPSS2	no	0.823	0.958	0.980
OMEGA-3	41_1.CUT	BPSS	yes	0.956	0.951	0.766
OMEGA-4	41_1.CUT	BPSS2	yes	0.894	0.910	0.975
OMEGA-5	41_1	BPSS	no	0.773	0.957	0.555
OMEGA-6	41_1	BPSS2	no	-	0.953	0.512
OMEGA-7	41_1	BPSS	yes	0.940	0.953	0.372
OMEGA-8	41_1	BPSS2	yes	0.450	0.954	0.982

Blind source separation on this data set has been initiated by using the JADE algorithm [46]. In particular, the 41_1 image of the permanent south polar region has been used for the supervised classification approach with WAVANGLET [39], unsupervised classification approach [47], and unsupervised blind source separation using BPSS [25]. Since no ground truth is available, the results from physical nonlinear inversion have been considered as a reference [39], [48], [49]. In this image, the surface is dominated by dust, and some spectra contain CO_2 and water ices (see Fig. 3). This reference data set for hyperspectral classification is available online.[1] The Luo *et al.* method introduced in [30] has estimated two sources

[1] http://sites.google.com/site/fredericschmidtplanets/Home/hyperspectral-reference

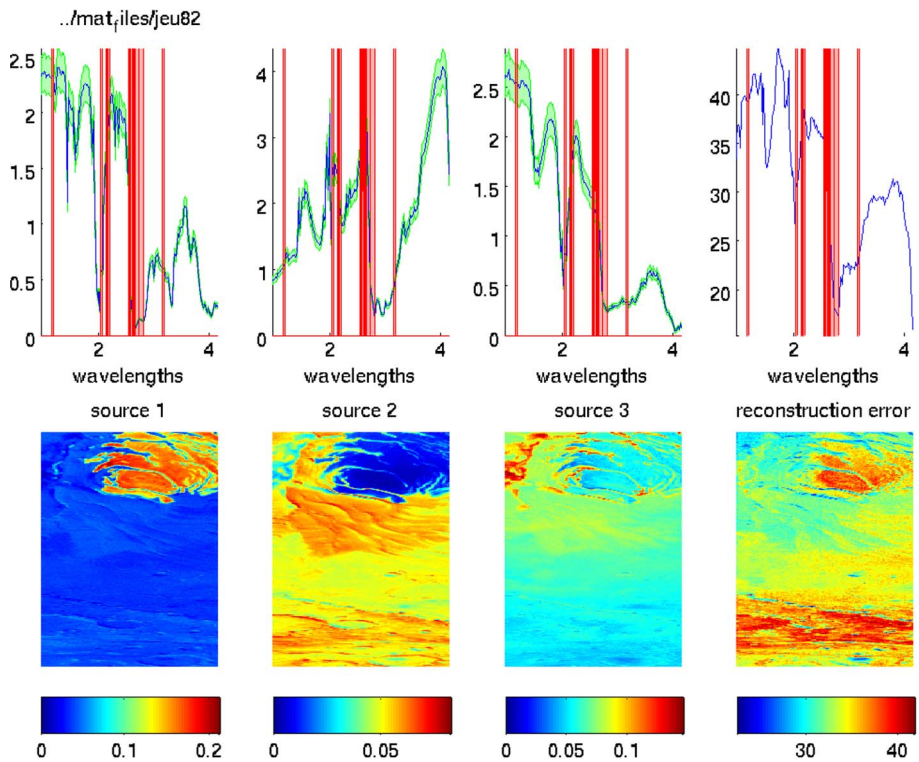

Fig. 4. Estimation of three sources of the entire OMEGA image 41_1 with BPSS using a preprocessing step of pixel selection employing the convex hull method. The first and third sources are clearly identified as CO_2 and H_2O ices (see Fig. 3) with correlation coefficients of 0.953 and 0.940, respectively (see run OMEGA-7 of Table VI). The spatial abundances are well estimated regarding the WAVANGLET classification method [39], [25]. The second source is identified as dust with a lower correlation coefficient (0.372).

for both 41_1 and 41_1.CUT images. From previous work using band ratio detection [41], physical inversion of the radiative transfer [48], [49], supervised classification approach using WAVANGLET [39], and unsupervised classification [47], three endmembers have been detected: dust, CO_2, and water ice. The number of sources has been tuned to three in our study.

The proportions of pixels containing CO_2 and H_2O ices on the 41_1 image are estimated to be 16.76% and 21.84%, respectively [39]. The first 300 lines of the 41_1 image (subset named 41_1.CUT) contain all spectra having ices. For this subset, the proportions of pixels with detected CO_2 and H_2O are 48.72% and 63.48%, respectively.

2) Performance: Computation times are about 100 times shorter when pixel selection by convex hull (CHO) has been performed as a preprocessing step (see Table V).

3) Accuracy: Table VI reports the results from different tests; each run is defined by a number. To estimate the quality of estimation, the correlation between the reference spectra and the estimated sources has been computed. The attribution of each source has been done *ad hoc* using both spectral source and spatial abundances.

a) Asymmetric abundances of the sources: The quality of estimation with both BPSS and BPSS2 is significantly lower for data set 41_1 (runs OMEGA-5 to OMEGA-8) in comparison with 41_1.CUT (runs OMEGA-1 to OMEGA-4). This result suggests that both BPSS and BPSS2 are less efficient in a case of an asymmetric distribution of the sources.

b) BPSS versus BPSS2: The BPSS algorithm gives significantly better results than the BPSS2 one (for instance, run OMEGA-3 versus OMEGA-4). This is due to nonlinearity in the radiative transfer and noise in the data set in contradiction with the full additivity constraint.

c) Effect of pixel selection: When convex hull selection has been used as a preprocessing step to BPSS/BPSS2, the estimation is significantly better (see Fig. 4 for run OMEGA-5 and Fig. 5 for run OMEGA-7). These results show that pixel selection is a way to better take into account the occurrence of rare endmembers and is thus an interesting method to provide better results.

V. Discussion and Conclusion

For the first time, an MCMC-based blind source separation strategy with positivity and sum-to-one constraints has been effectively applied on a complete hyperspectral image with a typical size frequently encountered in earth and planetary science. The optimization of BPSS [17] and BPSS2 [18] presented in this paper consists of two independent parts: 1) *TO* reduces the memory footprint, lowers the average cost of algorithmic operations, and makes smart reuse of memory, and 2) *CHO* reduces the number of spectra to process.

Fig. 6 summarizes the following results in a schematic form.

1) TO, for both BPSS and BPSS2, allows one to decrease the computation times by a factor of 1.5, without altering the accuracy of the results. Memory consumption has also been reduced by a significant factor. With such unambiguous advantages, the TO versions of BPSS and BPSS2 can be rather used than the original implementations.

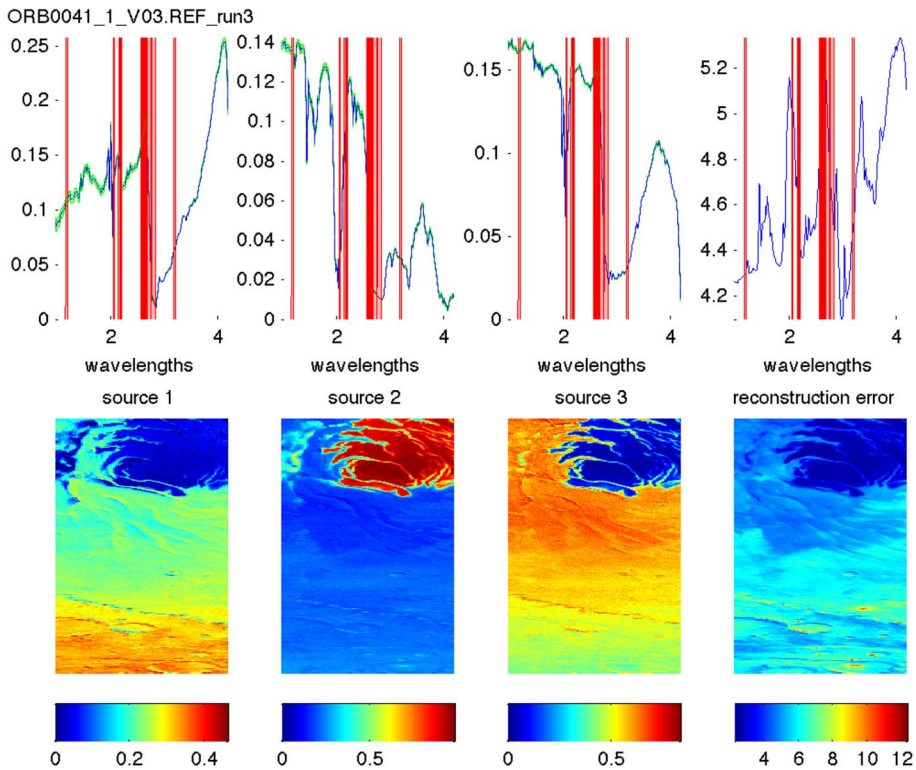

Fig. 5. Estimation of three sources of the entire OMEGA image 41_1 with BPSS without pixel selection. The second source is clearly identified as CO_2 ice (see Fig. 3) with a correlation coefficient of 0.957 (see run OMEGA-5 of Table VI). The first and third sources are identified as dust and water ice with lower correlation coefficients of 0.555 and 0.773, respectively. The spatial abundances of water ice are not well estimated regarding the WAVANGLET classification method [39].

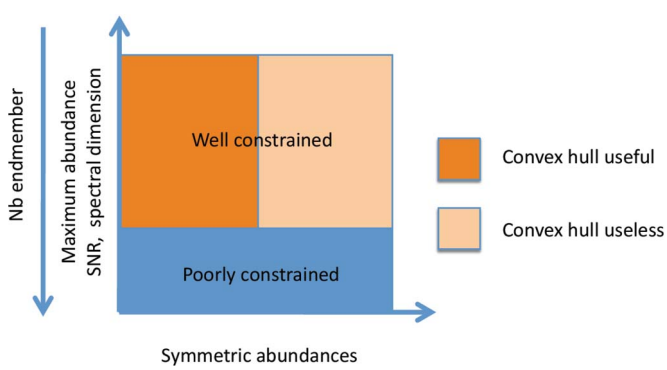

Fig. 6. Schematic of source separation estimation and usefulness of convex hull pixel selection for hyperspectral images.

2) Trivially, the results obtained for linear artificial data set (with uniform abundance distributions identical for each endmember with abundances until 100%) have demonstrated that the sources estimated by the TO strategy are equivalent to that by the CHO strategy (for instance, runs BPSS-1 to BPSS-2 in Table III and runs BPSS2-1 to BPSS2-2 in Table IV). In this case, pixel selection is still relevant to reduce the computation time by about 50 times (Table II).
3) The results obtained for the artificial data set with uniform abundance distributions and identical cutoffs for all endmembers have shown that the estimation of the sources is less accurate when a pixel selection (CHO) has been performed (runs BPSS-3 to BPSS-6 in Table III and runs BPSS2-3 to BPSS2-6 in Table IV). In this case, despite 50-times shorter computation times, using pixel selection as a preprocessing step seems to be inadequate.
4) For OMEGA data, the computation time reduction due to CHO has been around 100 (Table V). Abundance distributions can be significantly imbalanced (some endmembers are significantly less present in the scene). In that case, pixel selection by convex hull (CHO) is a way to overcome the bias caused by the overwhelming endmembers. This has been supported by the results obtained for the synthetic data set of linear mixture using imbalanced uniform distribution.
5) BPSS2 seems to better estimate the sources in the artificial data set but not in the real case. This is probably due to nonlinearity or the non-Gaussian noise effect.
6) The method BPSS2 appears to be very robust to Gaussian noise, as shown by the results obtained on the synthetic data set, even with 100-times actual OMEGA noise.
7) Sometimes, some sources have been well estimated but anticorrelated with the real spectra. This behavior has been interpreted to be due to the linearly dependent endmembers. In that case, spectra built by a linear combination of all sources except the considered source already contain spectral signatures of the considered source. The last source is then anticorrelated with the corresponding endmember to decrease his contribution. This behavior has to be studied in further detail because it is clearly a limitation of blind source separation.

In the future, the choice of the number of sources, which is an input in the current implementation, should be automated to allow one batch processing without human intervention. A methodology of pixel selection for use across data sets should also be established to enable integration of source separation techniques into larger systems and aim at the generation of catalogs and maps.

ACKNOWLEDGMENT

The authors would like to thank J. P. Bibring and the OMEGA Team for providing the OMEGA data set; S. Douté and B. Schmitt for their ice spectral library; the faculty of the European Space Astronomy Centre for the support; the Centre National d'Etudes Spatiales (CNES); the Programme National de Planétologie (CNRS/INSU); and the two anonymous reviewers for their valuable comments and suggestions that enabled significant improvements to this paper.

REFERENCES

[1] D. Tanre, M. Herman, P. Y. Deschamps, and A. de Leffe, "Atmospheric modeling for space measurements of ground reflectances, including bidirectional properties," *Appl. Opt.*, vol. 18, no. 21, pp. 3587–3594, Nov. 1979.

[2] G. Healey and D. Slater, "Models and methods for automated material identification in hyperspectral imagery acquired under unknown illumination and atmospheric conditions," *IEEE Trans. Geosci. Remote Sens.*, vol. 37, no. 6, pp. 2706–2717, Nov. 1999.

[3] N. Keshava and J.-F. Mustard, "Spectral unmixing," *IEEE Signal Process. Mag.*, vol. 19, no. 1, pp. 44–57, Jan. 2002.

[4] J. Scott, *Remote Sensing: The Image Chain Approach*. New York: Oxford Univ. Press, 1997.

[5] C.-I Chang, *Hyperspectral Data Exploitation: Theory and Applications*. New York: Wiley-Interscience, 2007.

[6] P. Comon, C. Jutten, and J. Hérault, "Blind separation of sources, Part II: Problems statement," *Signal Process.*, vol. 24, no. 1, pp. 11–20, Jul. 1991.

[7] A. Cichocki and S.-I. Amari, *Adaptive Blind Signal and Image Processing—Learning Algorithms and Applications*. New York: Wiley-Interscience, 2002.

[8] A. Hyvärinen, J. Karhunen, and E. Oja, *Independent Component Analysis*. New York: Wiley, 2001, ser. Adaptive and Learning Systems for Signal Processing, Communications, and Control.

[9] P. Paatero and U. Tapper, "Positive matrix factorization: A non-negative factor model with optimal utilization of error estimates of data values," *Environmetrics*, vol. 5, no. 2, pp. 111–126, Jun. 1994.

[10] D. D. Lee and H. S. Seung, "Learning the parts of objects by non-negative factorization," *Nature*, vol. 401, no. 6755, pp. 788–791, Oct. 1999.

[11] M. W. Berry, A. N. Langville, V. P. Pauca, and R. J. Plemmons, "Algorithms and applications for approximate nonnegative matrix factorization," *Comput. Stat. Data Anal.*, vol. 52, no. 1, pp. 155–173, Sep. 2007.

[12] M. Berman, H. Kiiveri, R. Lagerstrom, A. Ernst, R. Dunne, and J. F. Huntington, "ICE: A statistical approach to identifying endmembers in hyperspectral images," *IEEE Trans. Geosci. Remote Sens.*, vol. 42, no. 10, pp. 2085–2095, Oct. 2004.

[13] J. M. P. Nascimento and J. M. Bioucas-Dias, "Hyperspectral unmixing algorithm via dependent component analysis," in *Proc. IEEE IGARSS*, Jul. 2007, pp. 4033–4036.

[14] S. Jia and Y. Qian, "Spectral and spatial complexity-based hyperspectral unmixing," *IEEE Trans. Geosci. Remote Sens.*, vol. 45, no. 12, pp. 3867–3879, Dec. 2007.

[15] L. Miao and H. Qi, "Endmember extraction from highly mixed data using minimum volume constrained nonnegative matrix factorization," *IEEE Trans. Geosci. Remote Sens.*, vol. 45, no. 3, pp. 765–777, Mar. 2007.

[16] S. Jia and Y. Qian, "Constrained nonnegative matrix factorization for hyperspectral unmixing," *IEEE Trans. Geosci. Remote Sens.*, vol. 47, no. 1, pp. 161–173, Jan. 2009.

[17] S. Moussaoui, D. Brie, A. Mohammad-Djafari, and C. Carteret, "Separation of non-negative mixture of non-negative sources using a Bayesian approach and MCMC sampling," *IEEE Trans. Signal Process.*, vol. 54, no. 11, pp. 4133–4145, Nov. 2006.

[18] N. Dobigeon, S. Moussaoui, J.-Y. Tourneret, and C. Carteret, "Bayesian separation of spectral sources under non-negativity and full additivity constraints," *Signal Process.*, vol. 89, no. 12, pp. 2657–2669, Dec. 2009.

[19] W. Gilks, S. Richardson, and D. Spiegehalter, *Markov Chain Monte Carlo in Practice*. London, U.K.: Chapman & Hall, 1999.

[20] A. E. Gelfand and A. F. M. Smith, "Sampling based approaches to calculating marginal densities," *J. Amer. Stat. Assoc.*, vol. 85, no. 410, pp. 398–409, Jun. 1990.

[21] N. Bali and A. Mohammad-Djafari, "Bayesian approach with hidden Markov modeling and mean field approximation for hyperspectral data analysis," *IEEE Trans. Image Process.*, vol. 17, no. 2, pp. 217–225, Feb. 2008.

[22] M. Naceur, M. Loghmari, and M. Boussema, "The contribution of the sources separation method in the decomposition of mixed pixels," *IEEE Trans. Geosci. Remote Sens.*, vol. 42, no. 11, pp. 2642–2653, Nov. 2004.

[23] J. Nascimento and J. Dias, "Does independent component analysis play a role in unmixing hyperspectral data?" *IEEE Trans. Geosci. Remote Sens.*, vol. 43, no. 1, pp. 175–187, Jan. 2005.

[24] J. Wang and C.-I Chang, "Applications of independent component analysis in endmember extraction and abundance quantification for hyperspectral imagery," *IEEE Trans. Geosci. Remote Sens.*, vol. 44, no. 9, pp. 2601–2616, Sep. 2006.

[25] S. Moussaoui, H. Hauksdottir, F. Schmidt, C. Jutten, J. Chanussot, D. Brie, S. Douté, and J. Benediktsson, "On the decomposition of Mars hyperspectral data by ICA and Bayesian positive source separation," *Neurocomputing*, vol. 71, no. 10–12, pp. 2194–2208, Jun. 2008.

[26] J.-F. Cardoso and A. Souloumiac, "Blind beamforming for non Gaussian signals," *Proc. Inst. Elect. Eng.—F*, vol. 140, no. 6, pp. 362–370, Dec. 1993.

[27] A. Hyvarinen and E. Oja, "A fast fixed-point algorithm for independent component analysis," *Neural Comput.*, vol. 9, no. 7, pp. 1483–1492, Oct. 1997.

[28] C.-I Chang and Q. Du, "Estimation of number of spectrally distinct signal sources in hyperspectral imagery," *IEEE Trans. Geosci. Remote Sens.*, vol. 42, no. 3, pp. 608–619, Mar. 2004.

[29] J. M. Bioucas-Dias and J. M. P. Nascimento, "Hyperspectral subspace identification," *IEEE Trans. Geosci. Remote Sens.*, vol. 46, no. 8, pp. 2435–2445, Aug. 2008.

[30] B. Luo and J. Chanussot, "Unsupervised classification of hyperspectral images by using linear unmixing algorithm," in *Proc. IEEE ICIP*, Cairo, Egypt, 2009, pp. 2877–2880.

[31] C. B. Barber, D. Dobkin, and H. Huhdanpaa, "The quickhull algorithm for convex hulls," *ACM Trans. Math. Softw.*, vol. 22, no. 4, pp. 469–483, Dec. 1996.

[32] J. W. Boardman, "Analysis, understanding, and visualization of hyperspectral data as convex sets in n-space," *Proc. SPIE*, vol. 2480, pp. 14–22, 1995.

[33] C.-I Chang, C.-C. Wu, W.-M. Liu, and Y.-C. Ouyang, "A new growing method for simplex-based endmember extraction algorithm," *IEEE Trans. Geosci. Remote Sens.*, vol. 44, no. 10, pp. 2804–2819, Oct. 2006.

[34] J. Nascimento and J. Dias, "Vertex component analysis: A fast algorithm to unmix hyperspectral data," *IEEE Trans. Geosci. Remote Sens.*, vol. 43, no. 4, pp. 898–910, Apr. 2005.

[35] A. Ifarraguerri and C.-I Chang, "Multispectral and hyperspectral image analysis with convex cones," *IEEE Trans. Geosci. Remote Sens.*, vol. 37, no. 2, pp. 756–770, Mar. 1999.

[36] A. Plaza, P. Martinez, R. Perez, and J. Plaza, "A quantitative and comparative analysis of endmember extraction algorithms from hyperspectral data," *IEEE Trans. Geosci. Remote Sens.*, vol. 42, no. 3, pp. 650–663, Mar. 2004.

[37] M. Craig, "Minimum-volume transforms for remotely sensed data," *IEEE Trans. Geosci. Remote Sens.*, vol. 32, no. 3, pp. 542–552, May 1994.

[38] S. Douté and B. Schmitt, "A multilayer bidirectional reflectance model for the analysis of planetary surface hyperspectral images at visible and near-infrared wavelengths," *J. Geophys. Res.*, vol. 103, no. 12, pp. 31 367–31 390, Dec. 1998.

[39] F. Schmidt, S. Douté, and B. Schmitt, "WAVANGLET: An efficient supervised classifier for hyperspectral images," *IEEE Trans. Geosci. Remote Sens.*, vol. 45, no. 5, pp. 1374–1385, May 2007.

[40] R. N. Clark, G. A. Swayze, R. Wise, E. Livo, T. Hoefen, R. Kokaly, and S. J. Sutley, USGS Digital Spectral Library splib06a, U.S. Geological Survey, Reston, VA, 2007, [Online]. Available: http://speclab.cr.usgs.gov

[41] J.-P. Bibring, Y. Langevin, F. Poulet, A. Gendrin, B. Gondet, M. Berthé, A. Soufflot, P. Drossart, M. Combes, G. Bellucci, V. Moroz, N. Mangold, and B. Schmitt, "Perennial water ice identified in the south polar cap of Mars," *Nature*, vol. 428, no. 6983, pp. 627–630, Apr. 2004.

[42] S. Onn and I. Weissman, "Generating uniform random vectors over a simplex with implications to the volume of a certain polytope and to multivariate extremes," *Ann. Oper. Res.*, pp. 1–12, 2009. DOI: 10.1007/s10479-009-0567-7.

[43] G. Hughes, "On the mean accuracy of statistical pattern recognizers," *IEEE Trans. Inf. Theory*, vol. IT-14, no. 1, pp. 55–63, Jan. 1968.

[44] C. Lee and D. Landgrebe, "Analyzing high-dimensional multispectral data," *IEEE Trans. Geosci. Remote Sens.*, vol. 31, no. 4, pp. 792–800, Jul. 1993.

[45] J.-P. Bibring, A. Soufflot, M. Berthé, Y. Langevin, B. Gondet, P. Drossart, M. Bouyé, M. Combes, P. Puget, A. Semery, G. Bellucci, V. Formisano, V. Moroz, V. Kottsov, G. Bonello, S. Erard, O. Forni, A. Gendrin, N. Manaud, F. Poulet, G. Poulleau, T. Encrenaz, T. Fouchet, R. Melchiori, F. Altieri, N. Ignatiev, D. Titov, L. Zasova, A. Coradini, F. Capacionni, P. Cerroni, S. Fonti, N. Mangold, P. Pinet, B. Schmitt, C. Sotin, E. Hauber, H. Hoffmann, R. Jaumann, U. Keller, R. Arvidson, J. Mustard, and F. Forget, "OMEGA: Observatoire pour la Minéralogie, l'Eau, les Glaces et l'Activité," in *Mars Express: The Scientific Payload*. Noordwijk, The Netherlands: ESA Publications Division, Aug. 2004, pp. 37–49, ESA SP-1240.

[46] O. Forni, F. Poulet, J.-P. Bibring, S. Erard, C. Gomez, Y. Langevin, and B. Gondet, "Component separation of OMEGA spectra with ICA," in *Proc. 36th Annu. Lunar Planet. Sci. Conf.*, pp. 1623, S. Mackwell and E. Stansbery, Eds., Mar. 2005.

[47] L. Galluccio, O. J. J. Michel, P. Comon, E. Slezak, and A. O. Hero, "Initialization free graph based clustering," *IEEE Trans. Pattern Anal. Mach. Intell.*, 2009, submitted for publication.

[48] S. Douté, B. Schmitt, Y. Langevin, J.-P. Bibring, F. Altieri, G. Bellucci, B. Gondet, and F. Poulet, "South Pole of Mars: Nature and composition of the icy terrains from Mars Express OMEGA observations," *Planet. Space Sci.*, vol. 55, no. 1/2, pp. 113–133, Jan. 2007.

[49] C. Bernard-Michel, S. Douté, M. Fauvel, L. Gardes, and S. Girard, "Retrieval of mars surface physical properties from OMEGA hyperspectral images using regularized sliced inverse regression," *J. Geophys. Res.*, vol. 114, no. E6, p. E06 005, Jun. 2009.

Frédéric Schmidt received the Ph.D. degree from the Laboratoire de Planétologie de Grenoble (Centre National de la Recherche Scientifique (CNRS)–Université Joseph-Fourrier), Grenoble, France, in 2007.

He spent two years at the European Space Astronomy Centre, European Space Agency (ESA), Madrid, Spain, as a Postdoctoral Fellow. Since 2009, he has been an Assistant Professor with the Laboratoire Intéractions et Dynamique des Environnements de Surface, University Paris-Sud, Orsay, France, and is also with the Centre National de la Recherche Scientifique. He is a Coinvestigator of the OMEGA imaging spectrometer onboard Mars Express (ESA). His research interests are in analysis of hyperspectral data, ices, and polar processes on planet Mars.

Albrecht Schmidt received the Ph.D. degree from the University of Amsterdam, Amsterdam, The Netherlands, in 2002.

After working for three years at the University of Aalborg, Aalborg, Denmark, he joined the European Space Astronomy Centre, European Space Agency, Madrid, Spain, where he is currently a Computer Scientist with the Solar System Operations Division. His research interests are in data management and data analysis.

Erwan Tréguier received the Engineer degree from the École Nationale Supérieure d'Ingénieurs en Constructions Aéronautiques (currently part of the Institut Supérieur de l'Aéronautique et de l'Espace), Toulouse, France, in 2001 and the Ph.D degree from Université Paul Sabatier, Toulouse, in 2008, after defending his thesis in the Centre d'Étude Spatiale des Rayonnements.

He is currently holding a postdoctoral position at the European Space Astronomy Centre, European Space Agency, Madrid, Spain. His main field of research is planetary science. His research interests include the composition of the Martian surface (from both *in situ* and orbital data), geochemical modeling of alteration, and investigation of multidimensional data sets through statistical approaches.

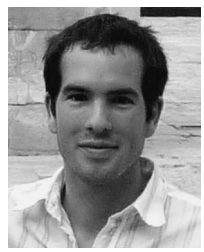

Maël Guiheneuf received the M.S. degree in signal processing from the École Centrale de Nantes, Nantes, France, in 2009.

He was a Student Fellow with the European Space Astronomy Centre, European Space Agency, Madrid, Spain, for six months in 2009 on the following subject: "Optimization strategies for hyperspectral unmixing using Bayesian source separation."

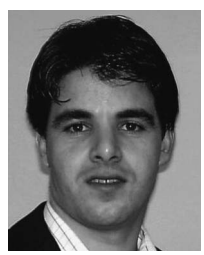

Saïd Moussaoui received the State Engineering degree from the École Nationale Polytechnique, Algiers, Algeria, in 2001 and the Ph.D. degree in automatic control and signal processing from Université Henri Poincaré, Nancy, France, in 2005.

He is currently an Associate Professor with the École Centrale de Nantes, Nantes, France, and since September 2006, he has been with the Institut de Recherche en Communication et Cybernétique de Nantes (IRCCyN), UMR CNRS 6597. His research interests are in statistical signal and image processing, including source separation, Bayesian estimation, and their applications.

Nicolas Dobigeon (S'05–M'08) was born in Angoulême, France, in 1981. He received the Engineering degree in electrical engineering from the Ecole Nationale Supérieure d'Electrotechnique, d'Electronique, d'Hydraulique et d'Informatique, et des Télécommunications, Toulouse, France, in 2004, and the M.Sc. and Ph.D. degrees in signal processing from the National Polytechnic Institute of Toulouse, Toulouse, in 2004 and 2007, respectively.

From 2007 to 2008, he was a Postdoctoral Research Associate with the Department of Electrical Engineering and Computer Science, University of Michigan, Ann Arbor. Since 2008, he has been an Assistant Professor with the National Polytechnic Institute of Toulouse (ENSEEIHT, University of Toulouse), within the Signal and Communication Group of the IRIT Laboratory. His research interests are focused on statistical signal and image processing, with particular interest in Bayesian inference and Markov chain Monte Carlo methods.